Available online at www.sciencedirect.com
SCIENCE DIRECT®
Combustion and Flame 146 (2006) 52–62
Combustion and Flame
www.elsevier.com/locate/combustflame

FT-IR and ^{1}H NMR characterization of the products of an ethylene inverse diffusion flame

Alexander Santamaría [a], Fanor Mondragón [a,*], Alejandro Molina [b], Nathan D. Marsh [c], Eric G. Eddings [c], Adel F. Sarofim [c]

[a] *Institute of Chemistry, University of Antioquia, A.A. 1226, Medellín, Colombia*
[b] *Combustion Research Facility, Sandia National Laboratories, Livermore, CA 94551, USA*
[c] *Department of Chemical Engineering, University of Utah, Salt Lake City, UT 84112, USA*

Received 26 August 2005; received in revised form 25 March 2006; accepted 4 April 2006

Available online 30 May 2006

Abstract

Knowledge of the chemical structure of young soot and its precursors is very useful in the understanding of the paths leading to soot particle inception. This paper presents analyses of the chemical functional groups, based on FT-IR and ^{1}H NMR spectroscopy of the products obtained in an ethylene inverse diffusion flame. The trends in the data indicate that the soluble fraction of the soot becomes progressively more aromatic and less aliphatic as the height above the burner increases. Results from ^{1}H NMR spectra of the chloroform-soluble soot samples taken at different heights above the burner corroborate the infrared results based on proton chemical shifts (Ha, Hα, Hβ, and Hγ). The results indicate that the aliphatic β and γ hydrogens suffered the most drastic reduction, while the aromatic character increased considerably with height, particularly in the first half of the flame.

Keywords: Soot; FT-IR; ^{1}H NMR; Inverse diffusion flame

1. Introduction

The intensive use of fossil fuels, mainly in combustion processes, leads to the generation of a carbonaceous material known as soot. Due to its high polyaromatic hydrocarbon content, this material even at low concentrations has serious consequences for human health, especially when the particulate matter is in the nanometer-sized range [1]. The health risks are not only mutagenic, but also potentially carcinogenic [1–4]. As a result, government agencies have introduced strict control measures that regulate the release of soot into the environment. Measures like these have encouraged research and development of environmentally friendly technologies [5–8].

The formation of soot is a very complex phenomenon that involves homogeneous and heterogeneous processes and continuous competition between reactions [9–12]. Although the process of soot evolution has been investigated experimentally and theoretically in many studies [8–44], there is still some information lacking on the chemical structure of the different compounds formed in the flame that lead to soot formation, especially during the early stages of soot

* Corresponding author. Fax: +57 4 210 6565.
E-mail address: fmondra@quimbaya.udea.edu.co (F. Mondragón).

0010-2180/$ – see front matter
doi:10.1016/j.combustflame.2006.04.008

inception. The acquisition of material with young soot characteristics represents an experimental challenge due to the fast oxidation and pyrolysis transformations that take place in the flame, especially in typical combustion systems [12,13,23,24]. To study the early period of soot formation, several types of diffusion flames have been used extensively, and one of these is the coflow normal diffusion flame (NDF) [8,12,18–21,33–35]. In the NDF, the fuel is introduced through the central tube of the burner while the oxidizer is introduced in an annular ring. An alternate approach is the inverse diffusion flame (IDF), which is basically obtained by inverting the air and fuel positions relative to a NDF configuration; that is, the oxidizer goes through the central tube and the fuel is in the annular space [22–32,35].

Up to now, most of the studies that involve the early period of soot formation have been carried out in normal diffusion flames due to their simplicity. Unfortunately, one of the disadvantages that this type of configuration presents is that soot particles and condensed intermediate hydrocarbons are transported toward the centerline of the flame due to thermophoretic forces. Because these particles are formed on the inner or fuel-rich side of the reaction zone, they must pass through the main reaction zone prior to exiting the flame, thus exposing them to significant oxidation and carbonization processes [12,23,33]. Therefore, obtaining young soot from this configuration requires intrusive sampling into the center of the flame, which results in disturbance of the system. Needless to say, the amount of sample obtained under these conditions is often minimal.

Studies carried out by Dobbins and colleagues in a NDF identified for the first time the presence of young soot in combustion systems, using thermophoretic particle deposition on a cooled target [19–21,33]. However, the results of this study were limited to transmission electron microscopy analysis due to the small amount of sample that could be collected. In another study using an underventilated normal diffusion flame configuration (U-NDF), a detailed analysis of young soot was obtained. Unfortunately, this type of configuration is somewhat difficult to operate in a reliable manner due to stability problems, which resulted in the flame being confined within the walls of a tube [34].

Although numerous investigations have been carried out on NDF configurations, very few have been done on an IDF. One of the first studies related to this type of configuration was published in 1955 by Arthur and Napier, who pointed out that the soot produced in an IDF was stickier and more viscous than the soot produced in a NDF [32]. However, it was only in 2002 that Blevins et al. confirmed that the soot generated in an IDF is chemically and morphologically similar to the young soot found in a U-NDF, with the characteristic that it is 50% soluble in dichloromethane, allowing direct chemical analysis [22,23].

Another advantage of the IDF configuration compared with NDF is that it provides a better separation of pyrolysis and oxidation processes. In addition, soot and intermediate products from these processes are transported away from the main reaction zone by thermophoretic forces, and since these products are formed on the outer or fuel-rich side of the flame, they do not pass through the main reaction zone and thus avoid significant oxidation or carbonization. This configuration provides an opportunity to gather large samples of young soot from the surroundings without need to invade the flame with the sampling probe. This approach opens the possibility of studying the early stages of soot formation in a direct way [22,23,25,27,28].

Although many experimental and theoretical investigations support the hypothesis that soot inception occurs through coagulation reactions of polycyclic aromatic hydrocarbons (PAHs) [10,13–17], which are formed quickly in the region of the flame just ahead of the nucleation zone (commonly defined as the onset of the yellow luminosity in a flame), very little is known about the molecular structure of these compounds. In particular, information on the variation of the content of oxygen and alkyl groups in PAH along the flame is missing and few studies in this direction have been carried out [36–39].

Recently, Öktem et al. [39] used photoionization aerosol mass spectrometry (PIAMS) to characterize semivolatile material present on soot particles deposited on an aluminum probe. The sample was collected at the soot inception region of a premixed ethylene flame. They found that at lower heights above the burner (below the soot inception point), the soot chemical composition was dominated by polycyclic aromatic hydrocarbons, whereas aliphatic compounds made a noticeable contribution to soot growth after the soot inception point, where the particles become older. Similar results were obtained by Ciajolo et al. [37,38] using FT-IR and UV–vis analyses. They found that the condensable material of soot collected in an ethylene premixed flame has a significant contribution of aliphatic hydrogens just after the soot inception point due to CH_2 and CH_3 groups. Although these studies were carried out on premixed flames, it should be noted that the current work reflects results from a diffusion flame.

One of the causes for the lack of structural information is that the spectroscopic characterization of these materials becomes difficult due to their low solubility in solvents, and the amount of sample, which that is often minimal. Therefore, much of the information available for premixed and diffusion flames

comes from solid state NMR and MS analyses [39, 42–44]. However, it is difficult to obtain detailed structural information from soot taken from these flames since, in general, significant carbonization or dehydrogenation has taken place.

The goal of this work is to provide detailed chemical information on the structural changes in the soluble fraction of soot obtained in an ethylene IDF, using spectroscopic techniques such as FT-IR and nuclear magnetic resonance of liquids.

2. Experimental

2.1. Burner

The IDF burner consists of three concentric brass tubes, which are distributed as follows: a central tube or air jet (1.2 cm i.d.), an intermediate tube used for supplying the ethylene as fuel (3.8 cm i.d.), and an outer tube (7.5 cm i.d.) for a N_2 stream that is used as a shield to prevent the formation of flames with the room air. The whole system is mounted on a screw-drive mechanism. The flow conditions for the gaseous system were set to 27, 117, and 289 cm^3/s for air, fuel, and N_2, respectively, so that the gas velocities at the burner mouth were 25 cm/s in all the experiments. Under these conditions the visible flame height was 60 mm and the maximum flame temperature was about 2100 K (see Fig. 1).

2.2. Sampling probe

Samples were taken at different heights on the lateral edge (6 mm radial position) from an ethylene IDF using a 10-cm-length stainless steel probe with a 1-mm-i.d. capillary tip. Initial experiments were carried out with a quartz probe to assess potential catalytic effects of the stainless steel probe, and results of both FT-IR and ^1H NMR analyses were equivalent, regardless of the sampling probe. Since the probe is sampling from the periphery of the flame and was thus at a significantly lower temperature than if it were sampling along the centerline. Thus stainless steel probe was used for experimental convenience.

The probe was connected to a vacuum system in line with a Teflon filter of 0.25-μm pore diameter that was used to collect the particulate matter and low-molecular-weight compounds that condense at 40 °C (the operating temperature of the heating tape). A cold trap was used to capture some of the volatile material that passed through the filter. The sampling time for each experiment depended on the amount of condensable sample, which was different at each sampling position, and varied from 20 min to 1 h. Generally, sampling at low flame positions required much more time than at higher positions because the particulate matter at this point was just forming.

The samples thus collected were extracted with chloroform using an ultrasonic bath at room temperature for 15 min. The soluble fraction was separated

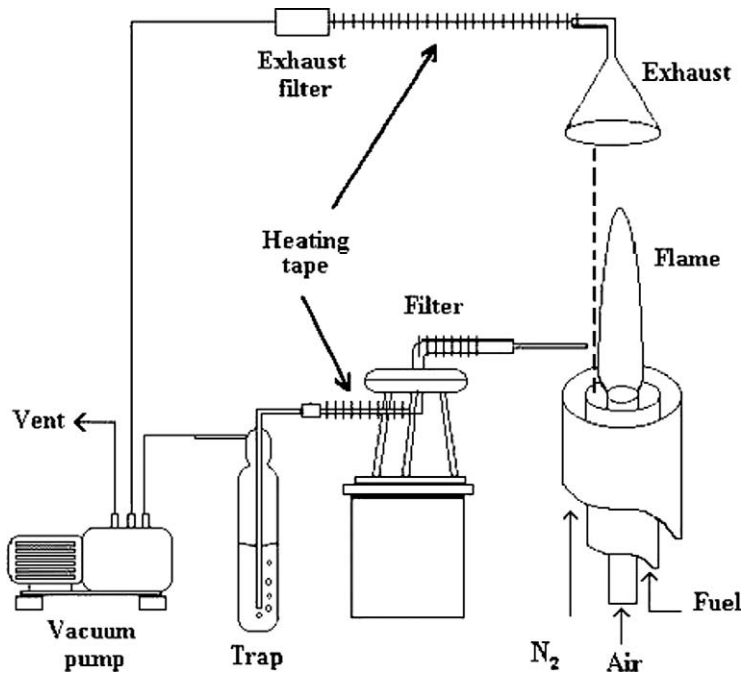

Fig. 1. Experimental setup of the IDF burner.

using a Teflon filter of 0.25-μm pore diameter. The chloroform was evaporated under an inert atmosphere using a vacuum stove at 60 °C.

2.3. FT-IR analysis

FT-IR spectra were taken of the combined sample, as well as of the chloroform soluble portion. It was observed that both spectra were very similar, which indicates that the IR signals are due predominantly to the structures present in the soluble material present in the soot particles. Therefore, the FT-IR analysis was carried out on the samples prior to chloroform extraction as described in the following paragraph.

A small amount of the total sample collected on the Teflon filter at heights of 6, 10, 15, 25, 30, 35, 45, and 60 mm and exhaust was taken to prepare a 1% KBr pellet. In each case, the sample and the KBr were dried at 60 °C under nitrogen before preparing the pellet. Each spectrum was the result of a 300-scan accumulation, a value that provided the best signal/noise ratio. A Nicolet Magna 560 spectrometer was used with a MCT/A detector operated in a wavelength range of 600–4000 cm^{-1}. Each sample was taken from the flame at least thrice to estimate reproducibility. The uncertainty of the IR measurements was less than 5%.

Table 1
Working conditions for ^{1}H NMR measurements

Frequency	300 MHz
Spectral width	3900 Hz
Memory capacity	32 K
Pulse width	9.60 μs
Acquisition time	1.0 s

2.4. ^{1}H NMR analysis

^{1}H NMR spectra of the chloroform soluble fraction of the samples collected on the filter at 6, 15, 35, and 45 mm and exhaust were taken. For the ^{1}H NMR experiments, the extracts were redissolved in $CDCl_3$ containing trace amounts of tetramethylsilane (TMS), which was used as an internal chemical shift reference to indicate in parts per million (ppm) the difference of the proton's resonance frequency. This is a number that gives information of the chemical environment of the protons in the sample. All spectra were taken in a Bruker AMX 300 spectrometer equipped with a 5-mm-inner-diameter tube and operated under conditions specified in Table 1.

Each spectrum was integrated manually at least four times and the results were averaged to reduce the uncertainty (less than 5%) generated by the manual adjustment. Then the spectrum of each sample was separated into characteristic regions for different protons (Ha, Hα, Hβ, and Hγ) according to their position in the molecule, using as a guide the chemical shifts assigned to characterize heavy crude oil ^{1}H NMR spectra [45–48]. See the corresponding ^{1}H NMR assignments in Table 2.

3. Results and discussion

3.1. FT-IR characterization

The infrared analysis was done on nine samples taken at different heights from the flame: 6, 10, 15, 25, 30, 35, 45, and 60 mm and exhaust. All FT-IR spectra showed C–H stretching features due to aromatic, aliphatic, and acetylenic groups. Fig. 2a shows a typical infrared absorption spectrum of the material collected in the filter at a height of 6 mm on the

Table 2
Assignments of the proton chemical shifts in NMR spectra

Hydrogens	Description	δ (ppm)
Ha	Aromatic hydrogens sterically hindered with bay, fjord regions and other geometrically similar zones. Aromatic hydrogens in very peri-condensed PAHs. Aromatic hydrogens corresponding to a single aromatic ring.	6.5–9.0
Hα	Aliphatic hydrogens in methylene groups α to two aromatic rings (fluorene type). Aliphatic hydrogens in methylene groups α to an aromatic ring and β position to another (acenaphthene type). Aliphatic hydrogens in methyl groups placed in bay or fjord regions of polyaromatic hydrocarbons.	2.0–5.0
Hβ	Alicyclic hydrogens in β position to two aromatic rings. Aliphatic hydrogens in methyl or methylene groups in β position to an aromatic ring.	1.0–2.0
Hγ	Aliphatic hydrogens in methyl groups γ or further to an aromatic ring.	0.5–1.0

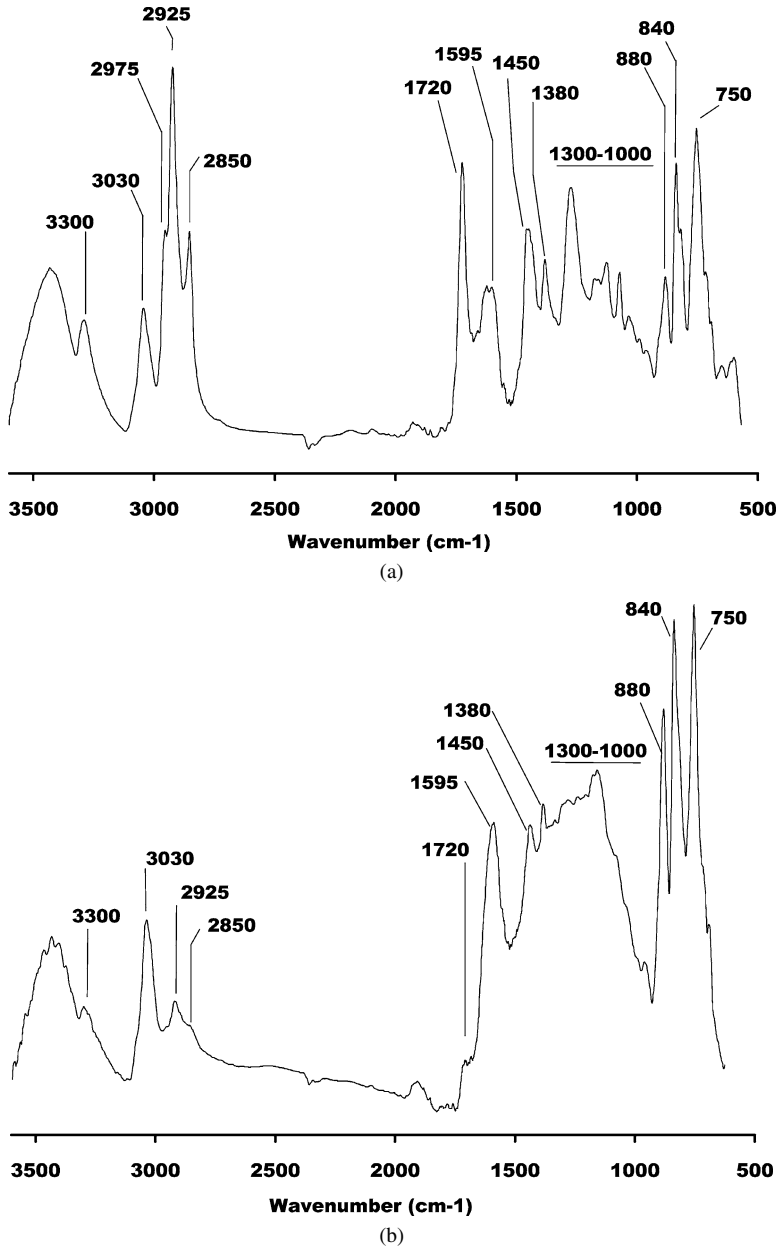

Fig. 2. Infrared spectrum of soot taken (a) at a 6-mm height in an ethylene IDF burner and (b) at the exhaust.

lateral edge of an ethylene IDF (see Table 3 for peak assignments).

This spectrum shows a sharp peak around 3300 cm^{-1} assigned to acetylenic C–H stretching groups, whose presence can partly sustain the hypothesis proposed by Frenklach et al. about the growth of polyaromatic units through the HACA mechanism [10, 13–17]. This mechanism basically consists of two repetitive steps: hydrogen abstraction from the reacting hydrocarbon by atomic hydrogen, followed by acetylene addition to the radical site formed. Under these conditions, the hydrogen and acetylene concentrations in the gas phase must be significant to be considered key species in the soot formation process. According to some previously published IDF experimental results [10,29,30], high concentrations of both hydrogen atoms and acetylene at the tip of the flame have been found; therefore, continuous alkylation reactions can take place.

Even though the sample in Fig. 2a was taken very low in the flame, a well-defined aromatic C–H stretching is observed at 3030 cm^{-1}, accompanied

Table 3
Assignment of infrared absorption peaks to functional groups

Absorption peaks (cm^{-1})	Assignments
3300	Acetylenic C–H stretching
3030	Aromatic C–H stretching
2975–2925–2850	Asymmetric and symmetric C–H stretching of CH_3, CH_2 aliphatic groups, respectively
1720	Carbonyl C=O stretching
1595	Aromatic and alkene C=C stretching
1450–1380	{ Asymmetric CH_3 and scissor CH_2 deformations Symmetric CH_3 deformation and cyclic CH_2
1300–1000	C–C and C–H plane deformation of aromatic groups and ether C–O–C stretching
890–840–750	C–H bending out of the plane of condensed aromatic systems

Table 4
Relative intensities of infrared absorption peak heights of soot generated in an ethylene IDF as a function of height above the burner

Height (mm)	Wavenumber (cm^{-1})									
	3300	3030	2975	2925	2850	1720	1620	880	840	740
6.0	0.422	0.388	0.533	1.000	0.529	0.656	0.357	0.393	0.696	0.758
10.0	0.608	0.934	0.556	1.000	0.533	0.603	0.801	0.963	1.896	2.050
15.0	0.726	1.046	0.588	1.000	0.593	0.336	0.778	1.082	2.042	2.085
25.0	1.129	1.603	0.671	1.000	0.553	0.028	1.802	3.000	4.612	4.235
30.0	1.076	1.675	0.640	1.000	0.614	0.0011	1.664	2.630	4.390	4.309
35.0	1.439	1.854	0.671	1.000	0.711	8.5E−4	2.471	2.844	4.561	4.464
45.0	1.404	2.350	0.723	1.000	0.733	5.3E−4	2.550	3.318	5.070	5.089
60.0	1.500	2.500	1.000	1.000	0.812	2.9E−4	2.812	4.875	7.250	7.375
Exhaust (200)	1.730	2.733	1.000	1.000	0.867	1.6E−4	3.526	6.333	7.667	8.200

Note. All data are normalized to the height of the 2925 cm^{-1} signal.

by the signals in the region from 1000 to 700 cm^{-1}. This region has three well-defined peaks corresponding to C=C–H out-of-plane deformation due to mono-, di-, and trisubstituted aromatic compounds and peri/cata-condensed aromatic rings. Generally, the peri-condensed aromatic compounds show infrared absorption peaks at 750, 840, and 850 cm^{-1}, whereas the cata-condensed aromatic compounds show absorption peaks at 750 and 850 cm^{-1}.

Concerning the presence of aliphatic structures, three characteristic sharp peaks assigned to aliphatic C–H stretching groups are seen at 2975, 2925, and 2850 cm^{-1}, respectively. The intermediate peak (2925 cm^{-1}) showed the most drastic change with the height of the flame. Therefore, it was used in the calculation of the relative intensities of the infrared absorption peak heights presented in Table 4, as was suggested by McKinnon et al. [36]. The presence of the C–H stretching in aliphatic groups comes mainly from methyl, methylene, and methine groups bonded to aromatic rings on PAHs or methylene bridges (fluorene type) maintaining the interconnection of PAHs within a network [12,36–38].

Fig. 2a also shows other characteristic signals in the region between 1720 and 1300 cm^{-1}, where the most important ones correspond to C=O stretching of carboxylic acids at 1720 cm^{-1} [36,40,41], C=C stretching of aromatic or alkene groups that appear at 1595 cm^{-1}, and aliphatic C–H plane deformations of CH_2/CH_3 groups at 1380 and 1450 cm^{-1}, respectively.

Fig. 2b shows the spectrum of the sample taken at the exhaust, which in general displays the same absorption peak pattern observed in Fig. 2a, with the exception of the signal at 1720 cm^{-1}, which disappears almost completely. This change is accompanied by the broadening of the region from 1000 to 1300 cm^{-1}, which is very significant. This region is a complex section of the infrared spectrum where signals corresponding to aromatic C–C and C–H plane deformation structures can appear, but the most important structures correspond to ether C–O–C stretching groups [40,41]. With the information currently available, however, a detailed analysis cannot be done.

Table 4 shows the variation in the relative intensity peaks for each spectrum normalized by the 2925 cm^{-1} aliphatic signal. In this way, we avoid making absolute peak height comparisons between different spectra which can be affected by factors such as the thickness and concentration of the KBr pellet. The most significant change in the data reported in

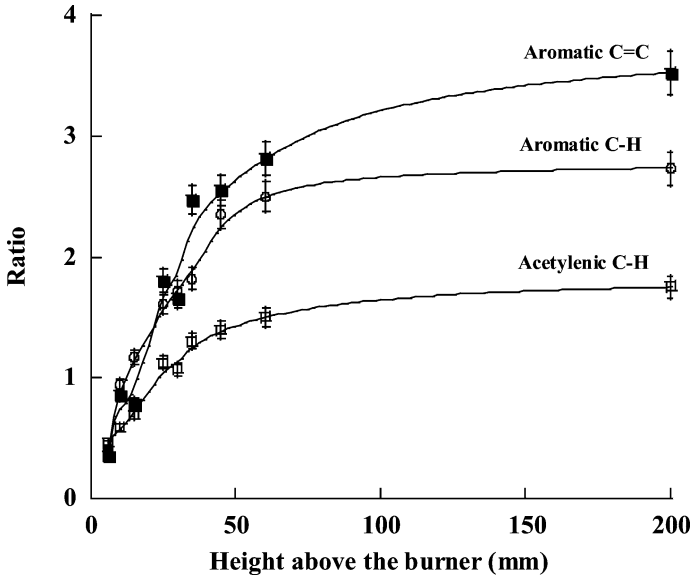

Fig. 3. Ratio of the C–H aromatic, C–H acetylenic, and C=C aromatic signals to aliphatic C–H stretch (2925 cm^{-1}) infrared absorption peak heights as a function of height above burner.

Table 4 was observed in the variation of the relative intensity of the aromatic (3030 cm^{-1}) to aliphatic (2925 cm^{-1}) C–H stretches as a function of height above the burner, whose ratio is plotted in Fig. 3. A significant increase of the aromatic and acetylenic relative ratio was observed during the first half on the flame, where there was a large temperature increase.

All samples showed the presence of carbonyl-type oxygenated functional groups (∼1720 cm^{-1}), which were more significant at the lower flame positions. The highest intensity of this signal was observed around 15 mm. Table 4 shows the variation of the ratio of carbonyl (1720 cm^{-1}) to aliphatic (2925 cm^{-1}) groups, where a drastic change in the signal at 1720 cm^{-1} appears at 25 mm, since the carbonyl group practically disappears. The origin of oxygenated functional groups in soot is not very clear and at the same time is not well documented in the scientific literature related to FT-IR analysis. Some authors have observed the presence of oxygenated groups in products of a laminar premixed flame by FT-IR (absorption peaks at 1700 and 3500 cm^{-1}) [36,40,41]. However, they state that it is very difficult to know whether these functionalities appear in situ or after sampling. In the present investigation, a clear trend with flame height was found, which suggests that these group of compounds may be involved in the soot formation process. However, one cannot rule out the possibility that the oxygen has been added in situ during sampling because the sampling probe is located near the interface of gaseous flows (air/fuel) where separation of the oxidation and carbonization processes is much more difficult to achieve, especially near the base flame. However, to remove this type of potential artifact is also difficult.

3.2. ^1H NMR characterization

^1H NMR analysis is a technique routinely used to characterize gasoline, heavy crude oils, and solvent-soluble coal fractions. The hydrogen groups associated with the chemical shift seen in ^1H NMR spectra can yield structural information that allows classification of complex mixtures containing hundreds of aromatic, naphthenic, paraffinic, olefinic, and isoparaffinic compounds [45–48].

Fig. 4a shows the ^1H NMR spectrum of the soluble fraction of soot obtained 6-mm above the burner. In the same figure, the different hydrogen types present in the sample are classified (see Table 2). The main assigned groups were hydrogen on aromatic rings (Ha, 6.5–9.0 ppm); hydrogen of CH, CH_2, CH_3 groups on carbon atoms in α position to aromatic rings (Hα, 2.0–5.0 ppm); hydrogen of CH, CH_2, CH_3 groups on carbon atoms in β position to aromatic rings (Hβ, 1.0–2.0 ppm); and methyl hydrogen on carbons γ, δ, or greater position to aromatic rings, as well as methyl hydrogen of alkanes, cycloalkanes, and naphthenic rings (Hγ, 0.5–1.0 ppm).

More detailed information on the chemical shifts observed by ^1H NMR is presented in Table 2. It is worth highlighting that the integration limits for hydrogens that belong to CH, CH_2, and CH_3 groups in a determined region of the spectrum are not easy to establish due to the high degree of signal overlap.

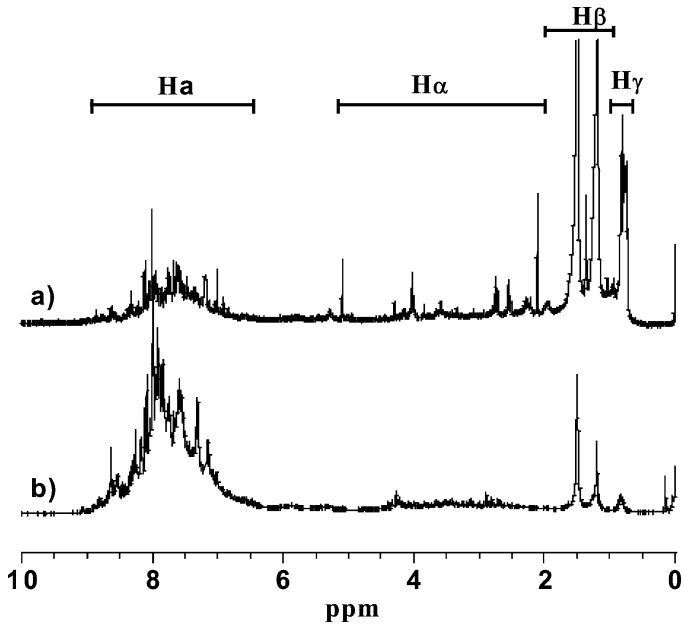

Fig. 4. ^{1}H NMR spectra of chloroform-soluble fraction of soot collected on the filter (a) at a 6-mm height in an ethylene IDF burner and (b) at the exhaust.

The sample collected at 6 mm was 94% soluble in chloroform. Its appearance was of an oily nature, very sticky and with a low softening point. At this point in the flame, there are gaseous species and tarry materials that can be identified as precursors of soot particles. These products have a significant aliphatic component with predominance of methyl and methylenic groups on β and γ positions to aromatic rings. It is important to observe that there is a significant fraction of hydrogen on the γ position between 0.7 and 0.8 ppm, which suggests the existence of large aliphatic chains or saturated rings (naphthenic-type) joined to different types of aromatic rings. The region between 3.5 and 5.0 ppm can correspond to olefinic hydrogens or CH_2 groups that connect two aromatic units (fluorene-type).

Fig. 4b shows the ^{1}H NMR spectrum of the chloroform soluble fraction (∼49%) of soot obtained in the exhaust. When compared with Fig. 4a, Fig. 4b shows a remarkable decrease of all the hydrogen signals of naphthenic, olefinic, and aliphatic character (chemical shift region between 0.5–6.0 ppm). This behavior corroborates the results obtained by FT-IR.

For comparative purposes, the region between 6.0 and 9.5 ppm of the spectra obtained at 6 mm and the exhaust was enlarged, as shown in Fig. 5. The chloroform-soluble fraction of the soot obtained in the exhaust shows a significant increase in the aromatic character as well as an increase in the condensation degree of aromatic units. Despite the complexity of the spectra, the degree of overlapping and the difficulty to assign signals to specific structures, the peaks in this region have been assigned as follows [45]: the region between 6.0 and 7.2 ppm has been assigned to hydrogens on a single aromatic ring; the region between 7.2 and 8.3 ppm has been assigned to hydrogens on diaromatic and most triaromatic and tetra-aromatic rings; the region between 8.3 and 8.9 ppm has been assigned to hydrogens on some tri- and tetra-aromatic rings; and the last region, 8.9–9.5 ppm, is assigned to hydrogens on tetra-aromatic rings or higher. Fig. 5 also shows that the soot soluble fraction obtained at 6 mm contains the same type of aromatic structures as found in the exhaust, although in a smaller concentration and with a different distribution. For example, in the exhaust the signal between 7.7 and 8.2 ppm is quite intense, indicating a greater amount of aromatic compounds of this type.

Fig. 6 shows a summary of the trends of each hydrogen type observed by ^{1}H NMR as a function of height above the burner. It can be observed that the aliphatic hydrogen fractions labeled as Hα, Hβ, and Hγ decrease with an increase in height above the burner, with the most drastic reduction evident with the β hydrogens (from 47.5 to 6.7%). This observation is accompanied by an increase in the aromatic hydrogen content (from 28 to 85.9%). These results indicate that the observed aliphatic structures early in the flame undergo dealkylation and/or cyclization reactions, leading to more compact structures.

The results described above seem to be contradictory to the results reported by Öktem et al. [39]

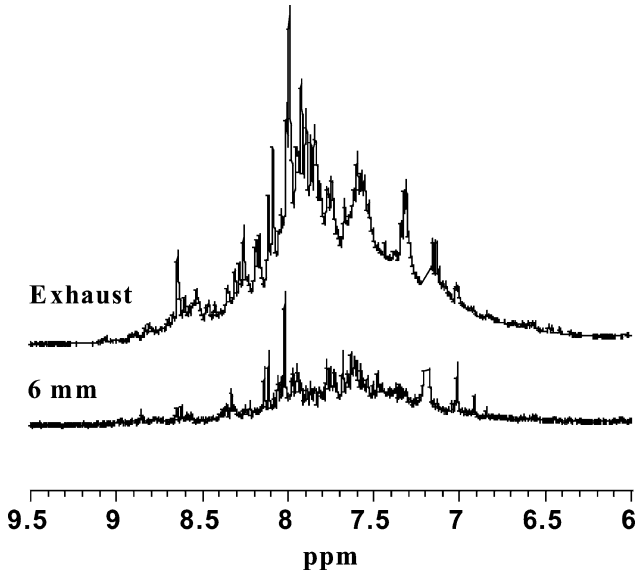

Fig. 5. Aromatic region enlargement of the ^{1}H NMR spectra of the chloroform-soluble fraction of soot.

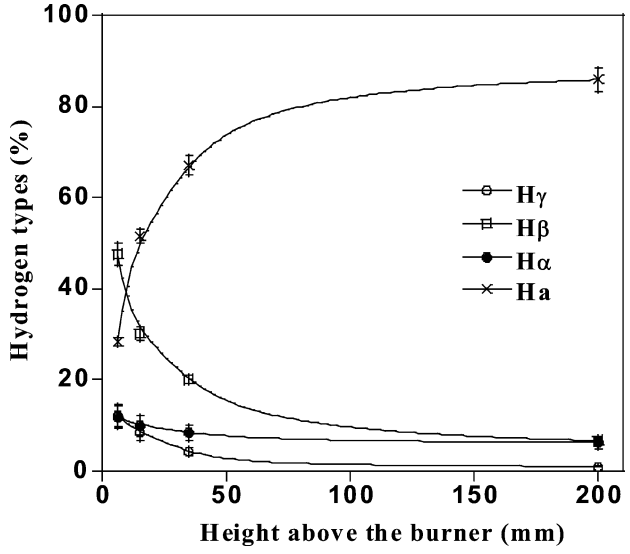

Fig. 6. Percentage variation of the different hydrogen types in the chloroform-soluble fraction of soot, based on the height above the burner.

and Ciajolo et al. [37,38]. However, this is not the case, since this study used a different flame configuration, where the carbonization and oxidation degrees are different from a premixed flame configuration. For a given nominal equivalent ratio, the soot collected from the periphery of an inverse diffusion flame (fuel-rich zone) would be less oxidized than the soot collected from a premixed flame. Thus, it is expected that soot and intermediate hydrocarbons produced in an inverse diffusion flame may have a different evolution history as height above the burner increases as compared to a premixed flame.

4. Concluding remarks

In the experiments reported in this work, FT-IR and ^{1}H NMR have given useful information on the molecular structure of soot precursors as a function of height above the burner surface in an ethylene inverse diffusion flame. Given that an IDF favors the collection of "young soot," the results of this research suggest that the soot formation process involves several general steps in the gaseous phase as well as in the condensed phase, accompanied by competing reactions among the original molecular fragments, tarry

materials and particles. The FT-IR spectra indicate that early in the flame the alkyl substituents are very important components of the tarry material. Similar results were obtained from ^{1}H NMR spectra of the chloroform-soluble fraction of soot, which is of an oily nature, very sticky, and with a low softening point and can be associated with the tarry components of the flame. Given the large content of the aliphatic structures observed by ^{1}H NMR in this fraction, it is very likely that, due to thermal effects, some of these aliphatic components may undergo bond scission, as observed by the drastic reduction of the β and γ hydrogens of CH_2 and CH_3 groups attached to aromatic rings. Such fragmentation produces more elemental molecular fragments, which may alkylate the tarry materials or the solid particles, and some of this material may rearrange to increase the quantity of aromatic components. The findings of this work may be useful in the development of theoretical soot evolution models, since many of the current models do not consider the contribution of the aliphatic species or decomposition reactions, which, according to the experimental results presented here, may be significant.

Acknowledgments

The authors thank the University of Antioquia for the financial support of the Sostenibilidad 2005 program. Useful comments of Mark Mikofski on the manuscript are acknowledged. A. Santamaría thanks Colciencias and the University of Antioquia for the Ph.D. scholarship and the Combustion Laboratory of the University of Utah for the visiting research grant in 2003.

References

[1] A.F. Sarofim, J.S. Lighty, E.G. Eddings, Prep. Symp. Am. Chem. Soc. Div. Fuel Chem. 47 (2) (2002) 618.
[2] C.J. Carrell, T.J. Carrell, H.L. Carrell, J.P. Glusker, E. Abu-Shaqara, C. Cortez, R.G. Harvey, Carcinogenesis 15 (11) (1994) 2931–2936.
[3] G.L. Borosky, J. Org. Chem. 64 (21) (1999) 7738–7744.
[4] Z. Zhou, Q. Dai, T. Gu, J. Chem. Inf. Comput. Sci. 43 (2) (2003) 615–621.
[5] H. Burtscher, Aerosol Sci. 36 (2005) 896–932.
[6] D.B. Kittelson, Aerosol Sci. 29 (5–6) (1998) 575–588.
[7] C.A. Miller, W.P. Linak, Primary Particles Generated by the Combustion of Heavy Fuel Oil and Coal, Report No. EPA-600/R-02-093, National Risk Management Research Laboratory, 2002.
[8] J.B. Moss, C.D. Stewart, Fire Safe. J. 30 (1998) 229–250.
[9] B.S. Haynes, in: W. Bartok, A.F. Sarofim (Eds.), Fossil Fuel Combustion, Wiley, New York, 1991, p. 261.
[10] M. Frenklach, Phys. Chem. Chem. Phys. 4 (11) (2002) 2028–2037.
[11] I.M. Kennedy, Prog. Energy Combust. Sci. 23 (1997) 95–132.
[12] K. Siegmann, K. Sattler, H.C. Siegmann, J. Electron Spectrosc. Relat. Phenom. 126 (2002) 191–202.
[13] A. Violi, G.A. Voth, A.F. Sarofim, Combust. Sci. Technol. 176 (2004) 1–14.
[14] A. D'Anna, A. Violi, A. D'Alessio, A.F. Sarofim, Combust. Flame 127 (1–2) (2001) 1995–2003.
[15] A. Violi, A.F. Sarofim, T.N. Truong, Combust. Flame 126 (1–2) (2001) 1506–1515.
[16] A. Violi, Combust. Flame 139 (4) (2004) 279–287.
[17] N.M. Marinov, W.J. Pitz, C.K. Westbrook, M.J. Castaldi, S.M. Senkan, Combust. Sci. Technol. 116–117 (1996) 211–287.
[18] F. Liu, H. Guo, G.J. Smallwood, O.L. Gulder, Combust. Theory Modelling 7 (2003) 301–315.
[19] R.A. Dobbins, R.A. Fletcher, H.C. Chang, Combust. Flame 115 (1998) 285–298.
[20] R.A. Dobbins, R.A. Fletcher, W. Lu, Combust. Flame 100 (1995) 301–309.
[21] R.A. Dobbins, H. Subremaniasivam, in: H. Bockhorn (Ed.), Soot Formation in Combustion, Mechanisms and Models, Springer-Verlag, Berlin, 1994, p. 290.
[22] L.G. Blevins, R.A. Fletcher, B.A. Benner, E.B. Steel, G.W. Mulholland, Proc. Combust. Inst. 29 (2002) 2325–2333.
[23] L.G. Blevins, N.Y. Yang, G.W. Mulholland, R.W. Davis, E.B. Steel, Prep. Symp. Am. Chem. Soc. Div. Fuel Chem. 47 (2) (2002) 740.
[24] V.R. Katta, L.G. Blevins, W.M. Roquemore, Combust. Flame 142 (2005) 33–51.
[25] C.R. Kaplan, K. Kailasanath, Combust. Flame 124 (1–2) (2001) 275–294.
[26] D.B. Makel, I.M. Kennedy, Combust. Sci. Technol. 97 (1994) 303–314.
[27] G.W. Sidebotham, I. Glassman, Combust. Sci. Technol. 81 (1992) 207–219.
[28] G.W. Sidebotham, I. Glassman, Combust. Flame 90 (1992) 269–283.
[29] K.T. Wu, R.H. Essenhigh, Proc. Combust. Inst. 20 (1984) 1925–1932.
[30] E.J. Lee, K.C. Oh, H.D. Shin, Fuel 84 (5) (2005) 543–550.
[31] K.C. Oh, U.D. Lee, H.D. Shin, E.J. Lee, Combust. Flame 140 (2005) 249–254.
[32] J.R. Arthur, D.H. Napier, Proc. Combust. Inst. 5 (1955) 303–315.
[33] R.A. Dobbins, C.M. Megaridis, Langmuir 3 (1987) 254–259.
[34] S. Leonard, G.W. Mulholland, R. Puri, R.J. Santoro, Combust. Flame 98 (1994) 20–34.
[35] L.R. Vander Wal, Proc. Combust. Inst. 26 (1996) 2269–2275.
[36] J.T. McKinnon, E. Meyer, J.B. Horward, Combust. Flame 105 (1996) 161–166.
[37] A. Ciajolo, B. Apicella, R. Barbella, A. Tregrossi, Proc. Combust. Inst. 27 (1998) 1481–1487.

[38] A. Ciajolo, R. Barbella, A. Tregrossi, L. Bonfanti, Combust. Sci. Technol. 153 (2000) 19–32.
[39] B. Öktem, M.P. Tolocka, B. Zhao, H. Wang, M.V. Johnston, Combust. Flame 142 (2005) 364–373.
[40] U. Kirchner, R. Vogt, C. Natzeckb, J. Goschnickb, Aerosol Sci. 34 (2003) 1323–1346.
[41] U. Kirchner, V. Scheer, R. Vogt, J. Phys. Chem. A 104 (2000) 8908–8915.
[42] R.J. Pugmire, M.S. Solum, Y.J. Jiang, A. F Sarofim, J. Veranth, H.H. Schobert, P.J. Pappano, Prep. Symp. Am. Chem. Soc. Div. Fuel Chem. 47 (2) (2002) 733–735.
[43] M.S. Solum, A.F. Sarofim, R.J. Pugmire, T.H. Fletcher, H. Zhang, Energy Fuels 15 (2001) 961–971.
[44] S. Yan, Y.J. Jiang, N.D. Marsh, E.G. Eddings, A.F. Sarofim, R.J. Pugmire, Energy Fuels 19 (2005) 1804–1811.
[45] M.D. Guillen, C. Diaz, C.G. Blanco, Fuel Process. Technol. 58 (1998) 1–15.
[46] S.W. Lee, B. Glavincevski, Fuel Process. Technol. 60 (1999) 81–86.
[47] Y. Yang, B. Liu, H. Xi, X. Sun, T. Zhang, Fuel 82 (2003) 721–727.
[48] G.S. Kapur, S. Berger, Fuel 81 (2002) 883–892.